ISSN 0915-633X

# NATIONAL INSTITUTE FOR FUSION SCIENCE

## A Monte Carlo Simulation Model for the Steady-State Plasma in the Scrape-off Layer

W.X.Wang, M. Okamoto, N. Nakajima,
S. Murakami and N. Ohyabu

(Received - Nov. 22, 1995 )

NIFS-391 Dec. 1995

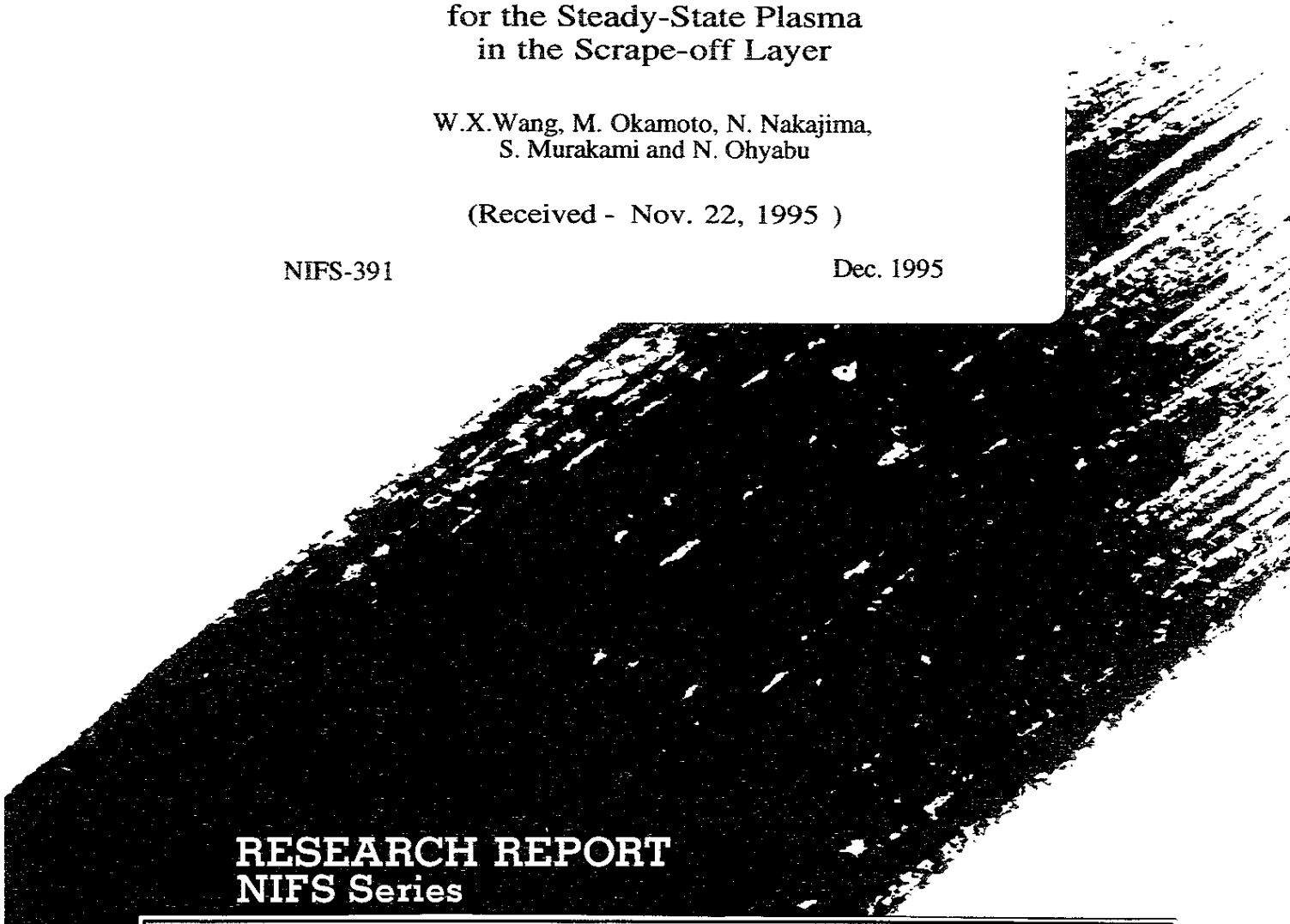

**RESEARCH REPORT**
**NIFS Series**



NAGOYA, JAPAN

# A Monte Carlo Simulation Model for the Steady-State Plasma in the Scrape-off Layer

W. X. WANG[†], M. OKAMOTO[†,‡], N. NAKAJIMA [†,‡],
S. MURAKAMI[†,‡], N. OHYABU[†,‡]

[†]Department of Fusion Science, The Graduate University for Advanced Studies,

Nagoya 464-01, Japan

[‡]National Institute for Fusion Science,

Nagoya 464-01, Japan

**Abstract**

A new Monte Carlo simulation model for the scrape-off layer ( SOL ) plasma is proposed to investigate a feasibility of so-called "high temperature divertor operation". In the model, Coulomb collision effect is accurately described by a nonlinear Monte Carlo collision operator; a conductive heat flux into the SOL is effectively modelled via randomly exchanging the source particles and SOL particles; secondary electrons are included. The steady state of the SOL plasma, which satisfies particle and energy balances and the neutrality constraint, is determined in terms of total particle and heat fluxes across the separatrix, the edge plasma temperature, the secondary electron emission rate, and the SOL size. The model gives gross features of the SOL such as plasma temperatures and densities, the total sheath potential drop, and the sheath energy transmission factor. The simulations are performed for collisional SOL plasma to confirm the validity of the proposed model. It is found that the potential drop and the electron energy transmission factor are in close agreement with theoretical predictions. The present model can provide primarily useful information for collisionless SOL plasma which is difficult to be understood analytically.

**Keywords**: Monte Carlo simulation, scrape-off layer plasma, Debye sheath, conductive heat flux.

# 1. INTRODUCTION

Toroidal devices employ a divertor configuration for the purpose of particle and heat control. The magnetic field separatrix in the divertor configuration separates a narrow boundary layer or scrape-off layer ( SOL ) from the confinement region. Since the SOL has no closed and nested magnetic surfaces, the plasma behaves differently in the SOL from in the confinement region. Charged particles in the SOL are guided along open magnetic field lines rapidly to the divertor plates. The Debye sheaths [1,2] are formed just in front of the divertor plates to maintain ambipolar particle fluxes to the plates. Electric potential well due to the formation of Debye sheaths characterizes the plasma behavior in the SOL. Atomic processes of neutral atoms and impurity ions in the divertor region play an important role in determining particle recycling and heat removal.

Recently, scenarios of high temperature divertor operation have been proposed [3]. This operation requires a collisionless plasma in the SOL and strong pumping in the divertor region. It is essential in this operation mode with high temperatures that the plasma should not be cooled due to secondary electrons emitted from the divertor plates.

Potential formation in the boundary layer plasma or in the SOL has been investigated related to the plasma-surface interaction. Conventional analyses [4-15], as well as some numerical simulations [16-18], assumed that electrons obey a Maxwell-Boltzmann distribution, and kinetic models [4-12] further assumed that ions are Coulomb collision-free. However, the Coulomb collisionality of the SOL plasma can vary over a wide range and the particle velocity distribution function may be distorted a great deal from the Maxwellian. The improvement was made by the particle simulations [19-21] with collisional kinetic treatment on both ions and electrons. In these simulations, the secondary electron emission was not included.

In understanding characteristics of the SOL plasma in tokamaks or helical systems, it is essential to determine the sheath potential, the plasma temperature and density, secondary electron effect, and sheath energy transmission factor consistently with particle and energy flows from the confinement region to the SOL. Coulomb collisions play an important role in determining whether or not particles cross the potential barrier. Since self-collisions are important and the plasma may have a velocity distribution far from a Maxwellian, a nonlinear collision operator should be used for this problem.

In this paper, we present a new Monte Carlo particle simulation model for the SOL

plasma, to investigate a feasibility of the high temperature divertor operation. In the model, particle dynamics is not followed assuming a steady-state uniform plasma along the magnetic field lines. This simplification results from the fact that fast streaming of the particles along magnetic field lines outweighs the perpendicular diffusion in determining the SOL structure. Simulations based on the presented model are performed in the velocity space. The cross-field plasma transport into the SOL and the secondary electron emission from the plates are treated as the sources, and the particle and energy sink effects due to the plates are introduced through the field length $L$ between the two divertor plates. The steady state of the SOL plasma and the sheath potential are determined by the requirement of particle flux balance, energy balance and charge neutrality constraint. The steady state depends upon, parametrically, the total particle flux across the separatrix into the SOL $\Gamma_a^t$ ( hereafter subscript $a = e, i$, denotes either electrons or ions ), input power $Q_a^{in}$, the size of the SOL, ( i.e, the length of magnetic field lines between the two divertor plates $L$ and the SOL volume $V_{SOL}$ ), the temperatures of main plasma near the separatrix $T_{sa}$, and the secondary electron emission rate $\delta_e$. In the present model, atomic processes such as charge exchanges, ionizations, recombinatons of neutral atoms and impurity ions are not taken into account. However, within the framework of the above simplification, the model can clarify the essential characteristics of a general SOL system.

A nonlinear Monte Carlo collision operator[22], which has been developed to implement Landau collision integral[23], is employed to describe Coulomb collision effect in the simulation model. We can accurately simulate Coulomb collisions even if the SOL plasma deviates far from a Maxwellian distribution. The conductive energy flux from the confinement region into the SOL, which has not been included in the previous work based on the model Fokker-Planck equation[24], is newly included in addition to the convective energy flux to ensure integrated balance of energy flowing to the SOL and energy lost to the divertor plates. This conductive energy flux can not be neglected in self-consistent determination of the SOL structure. A special heat source is added to the model Fokker-Planck equation to simulate the conductive energy flux as a first trial. The secondary electron emission due to plasma-surface interaction, which may significantly affect the SOL system, is also included in the model.

The description of the model is given in detail in Section 2. In Section 3, the model is applied to collisional SOL plasma, in which the electron mean-free path $\lambda_e$ is shorter than

the system connection size $L$, and the simulation results are shown and compared to the theory. In Section 4, conclusions are summarized.

# 2. DESCRIPTION OF THE MODEL

In describing the SOL plasma, we employ a simple one dimensional system parallel to the magnetic field illustrated in Fig. 1. The plasma particles diffusing across the separatrix from the confinement region into the SOL, flow along the magnetic field lines toward the divertor plates. The potential sheaths with the width of a few Debye lengths are formed just in front of the two divertor plates as a negative potential well with the height of $-\Phi$ ($\Phi < 0$) for electrons in the SOL. The electrons with parallel kinetic energy less than the potential energy ( $\frac{1}{2}m_e v_\parallel^2 < -e\Phi$ ) are trapped and bounce between the two divertor plates and the electrons with parallel kinetic energy larger than the potential energy ( $\frac{1}{2}m_e v_\parallel^2 > -e\Phi$) can cross the barriers onto the plates. On the other hand, all ions can freely penetrate the sheaths onto the plates. Since the parallel flow is much faster than the perpendicular diffusion across the magnetic field lines, we assume that the plasma is uniform along the magnetic field lines neglecting drifts of the particles across the field lines. Under the above consideration, we employ the point model, in which the distribution function $f_a(\vec{v}, t)$ evolves only in the velocity space as

$$\frac{\partial f_a(\vec{v}, t)}{\partial t} = C(f_a) + \text{sources/sinks}, \tag{1}$$

to describe the SOL plasma. Here $a$ denotes the $a$-species ( electrons or ions ) and $C(f_a)$ is the Coulomb collision operator. The model is established in the velocity space. To consider the perpendicular fluxes across the separatrix into the SOL, the particle loss through the sheath to the divertor plates and the secondary electron emission, some sources and sinks are introduced in the model equation to convert these spatial effects into the velocity space. Before presenting the concrete form of the sources and sinks, we explain the basic consideration for modeling the SOL plasma as follows.

1) The particle injection model [19,21], which introduces source particles with some velocity distribution into the system at a given rate, is used to simulate the particle flux across the separatrix from the confinement region into the SOL. Particle sources for electrons and ions, $S_{pe}$ and $S_{pi}$, respectively, are included in the model equation.

2) If the particles flowing along the magnetic field lines penetrate the potential barrier and reach the divertor plates, they are regarded to be lost. Thus, the plates act as strong particle and energy sinks for the plasma. A particle life time $\tau_{\|a}$ is defined as the transit time along the magnetic field line to the plates

$$\begin{aligned} \tau_{\|e} &= \begin{cases} \infty, & \text{for trapped electrons} \quad \left(\frac{1}{2}mv_{\|}^2 \leq -e\Phi\right) \\ L/2|\vec{v}_{\|}|, & \text{for untrapped electrons} \quad \left(\frac{1}{2}mv_{\|}^2 > -e\Phi\right) \end{cases} \\ \tau_{\|i} &= \frac{L}{2|\vec{v}_{\|}|}, \qquad \text{for all ions (untrapped)} \end{aligned}$$

to describe these sinks, where $L$ is the SOL system size, i.e, the length of magnetic field lines between the two divertor plates.

3) Secondary electrons are born on the plates with typical kinetic energy of a few $eV$, and then accelerated by the sheath potential to have parallel kinetic energy of about $-e\Phi$. In the Fokker-Planck simulations by a finite difference method [16,18,24], it is rather difficult to include secondary electrons because they are highly localized in the velocity space. However, in the present Monte Carlo particle simulation, one can easily treat secondary electrons by using the particle injection method. The source for secondary electrons $S_{2e}$ is added in the model equation.

4) The cross-field energy flux (or conductive energy flux) into the SOL is independent of the particle flux in determining the structure of the SOL, because the energy flux consists of convective part brought by the particle flux, as well as conductive part. Maintaining the integrated energy balance in the SOL is essential to evaluate correct heat flux onto the divertor plates. The power load on the divertor plates has attracted much attention in the design of large fusion devices since the heat removal capability of current divertor plate is limited. The total kinetic energy flux $\vec{q}^{\text{tot}}$ across the separatrix into the SOL includes contribution from both convective and conductive processes. It is defined as

$$\begin{aligned} \vec{q}^{\text{tot}} &\equiv \int \vec{v}_{\perp}\frac{mv^2}{2}f_s(\vec{v})d^3v \\ &= \vec{q}^{\text{conv}} + \vec{q}^{\text{cond}}, \end{aligned} \tag{2}$$

where $\vec{q}^{\text{conv}}$ and $\vec{q}^{\text{cond}}$ are the convective and conductive flux, respectively,

$$\vec{q}^{\text{conv}} \equiv \int \langle \vec{v}_{\perp} \rangle \frac{mv^2}{2} f_s(\vec{v})d^3v, \tag{3}$$

$$\vec{q}^{\rm cond} \equiv \int (\vec{v}_\perp - \langle \vec{v}_\perp \rangle) \frac{mv^2}{2} f_s(\vec{v}) d^3v$$
$$\simeq \kappa_\perp \nabla_\perp T_s, \tag{4}$$

$f_s(\vec{v})$ and $T_s$ are , respectively, the distribution function and temperature on the separatrix, and $\kappa_\perp$ is the thermal conductivity which is dominated by anomalous transport. Particle source term only contributes to the convective part of the energy flux. The energy balance in the SOL can be expressed as

$$Q^{\rm in} = \int_{S_A} \vec{q}^{\rm tot} \cdot d\vec{S} = Q^{\rm loss}, \tag{5}$$

where $Q^{\rm in}$ is the input power and $Q^{loss}$ is loss power due to particle incidence on the plates. The integration is performed over the separatrix surface $S_A$. To maintain Eq.(5), conductive energy flux should be considered. It should be noted that since usually $\vec{q}^{\rm cond} > \vec{q}^{\rm conv}$, the lack of the conductive heat source term may lead to a incorrect result in a study. For the sake of correct evaluation of the power loading and the rationality of the model itself, a new source term, which gives rise to only conductive heat flux, is included in the model equation. This newly added term is not considered in the previous model[24]. In the present model, the heat source $S_{qa}$ is incorporated by the method of particle exchange between the SOL plasma and the source plasma originated from the confinement region. This term simulates conductive energy flux for the balance of input power, but it does not give rise to an extra particle flux.

We now express the Fokker-Planck equations which evolve electron and ion velocity distribution functions, $f_e(\vec{v})$ and $f_i(\vec{v})$, respectively, to steady state,

$$\frac{\partial f_e}{\partial t} = C(f_e) - \frac{f_e}{\tau_{\|e}} H(|\vec{v}_\|| - v_c) + S_{pe} + S_{2e} + S_{qe}, \tag{6}$$

$$\frac{\partial f_i}{\partial t} = C(f_i) - \frac{f_i}{\tau_{\|i}} + S_{pi} + S_{qi}. \tag{7}$$

Here $C(f_e)$ and $C(f_i)$ are nonlinear self-collision operators.

The second term on the right side of Eq.(6) describes electron loss to the plates due to untrapped electrons overcoming the sheath potentials, in which $H(|\vec{v}_\|| - v_c)$ is the Heaviside step function and $v_c = \sqrt{-2e\Phi/m_e}$.

The source terms $S_{pa}(\vec{v})$ in Eqs.(6) and (7) used to simulate the particle flux from the confinement region into the SOL depend on the main plasma distribution near the separatrix and complicated cross-field particle transport. It is not evident what the source

velocity distribution actually is. A simple one is Maxwellian source [10,24], which is used in the simulation presented in next section, given by

$$S_{pa} = \dot{S}_a \frac{\exp(-v^2/v_{sa}^2)}{\int \exp(-v^2/v_{sa}^2) d^3v}, \tag{8}$$

where $v_{sa} = \sqrt{2T_{sa}/m_a}$ with $T_{sa}$ defined as source temperature which may be considered as the main plasma temperature very near the separatrix. The source strength $\dot{S}_a$ relates to the total particle flux across the separatrix $\Gamma_a^t$ as follows

$$\Gamma_a^t \equiv \int_{S_A} \vec{\Gamma}_a \cdot d\vec{S} = \int_{V_{SOL}} d^3x \int d^3v S_{pa} = V_{SOL} \dot{S}_a, \tag{9}$$

where $\vec{\Gamma}_a$ is the particle flux and $\int_{V_{SOL}} d^3x$ is the space integration over the whole SOL volume $V_{SOL}$. One can use Eq.(9) to specify $\dot{S}_a$ assuming that $\Gamma_a^t$ and $V_{SOL}$ are known. The ambipolarity of the cross-field flux implies $\dot{S}_i = \dot{S}_e$.

The secondary electron emission term in Eq.(6) is expressed as

$$S_{2e} = \delta_e \int \frac{f_e}{\tau_{\|e}} H(|\vec{v}_\|| - v_c) d^3v \cdot \frac{g(\vec{v})}{\int g(\vec{v}) d^3v}, \tag{10}$$

where $\delta_e$ is the emission rate. Secondary electrons are generated on the plates with kinetic energy of a few $eV$ and accelerated by the sheath potential. Since the structure of the sheath is neglected in the present model, $g(\vec{v})$, the velocity distribution function for secondary electrons as a source in Eq.(6), can be reasonably set as

$$g(\vec{v}) = \exp\left(-\frac{m_e v_\perp^2}{2T_{2e\perp}}\right) \frac{\delta(v_\| - v_c) + \delta(v_\| + v_c)}{2} \tag{11}$$

with $T_{2e\perp} \sim$ a few $eV$.

The conductive heat source is taken as

$$S_{qa} = \dot{S}_{qa} \left( \frac{\exp\left(-v^2/v_{sa}^2\right)}{\int \exp\left(-v^2/v_{sa}^2\right) d^3v} - \frac{f_a}{\int f_a d^3v} \right). \tag{12}$$

Integration of Eq.(12) multiplied by $m_a v^2/2$ over the velocity space and the SOL volume yields a conductive heat flux into the SOL

$$\bar{q}^{\text{cond}} = \frac{3}{2} \dot{S}_{qa} (T_{sa} - T_a) \frac{V_{SOL}}{S_A},$$

with the effective temperature $T_a$ defined by $\frac{3}{2}T_a = \int \frac{1}{2}m_a v^2 f_a(\vec{v})d^3v$. This heat flux results from randomly exchanging the source particles coming from the confinement region and the SOL particles according to the rate $\dot{S_{qa}}$. It gives

$$\bar{q}^{\text{cond}} = \frac{\kappa_\perp}{\Delta_s}(T_{sa} - T_a)$$

if the exchange rate takes $\dot{S_{qa}} = \frac{2}{3}\frac{\kappa_\perp}{\Delta_s^2}$, where $\Delta_s$ is the thickness of the SOL. Note that integration of Eq.(12) over the velocity space shows that $S_{qa}$ gives no particle flux and hence no convective heat energy.

In the present model, Coulomb collisions are treated in the Fokker-Planck approximation. The quantity which measures the collisionality of the SOL system is defined as the ratio of $L/2$ to the particle mean-free path in the parallel direction $\lambda_a$, i.e, $L/(2\lambda_a)$, where $\lambda_a = \tau_{aa}\sqrt{2T_{a\|}/m_a}$ ($\tau_{aa}$ is the like-particle equilibration time[25] and $T_{a\|}$ is the parallel temperature). The collisionality can range from an extremely small value to a very large value in different operation modes. The distribution function of the SOL plasma, especially in high temperature operation mode, may significantly deviates from the Maxwellian. In a particle model, Coulomb collisions can be implemented by a Monte Carlo operator. The linear operators describe Coulomb collisions by following test particles under a Maxwellian background, and therefore, can not well fulfill the application here since, as mentioned above, the distribution function of the SOL plasma may be far from the Maxwellian. We have developed a nonlinear Monte Carlo collision operator[22] which removed the assumption of a Maxwellian background by colliding all particles each other. In the nonlinear operator, the Coulomb effect is incorporated by a number of elastic binary collisions as follows.

At each integration step of time interval $\Delta t$ all particles are randomly paired, or grouped and then paired for collisions. The velocity change of a particle $a$ ($m_a$, $\vec{v}_a$, $e_a$) ( the quantities shown in parentheses are the mass, velocity and charge of the particle, respectively) during a binary collision with a particle $b$ ($m_b$, $\vec{v}_b$, $e_b$) is determined by

$$\Delta\vec{v}_a = \frac{m_b}{m_a + m_b}[(\sin\epsilon)\hat{n} \times \vec{u} + (1 - \cos\epsilon)\hat{n} \times \hat{n} \times \vec{u}], \tag{13}$$

where the small parameter $\epsilon$ is given by

$$\frac{\epsilon^2 u^3}{3} = \Delta t(4\pi e_a^2 e_b^2 \ln\Lambda)\left(\frac{1}{m_a} + \frac{1}{m_b}\right)^2 \gamma, \tag{14}$$

$\vec{u} = \vec{v}_a - \vec{v}_b$ is the relative velocity before the collision, $\ln\Lambda$ is the Coulomb logarithm, and $\hat{n}$ is a random unit vector with uniform distribution. The factor $\gamma$ in Eq.(14) takes

$$\gamma = \begin{cases} \dfrac{n_b}{N_b} = \dfrac{n_a}{N_a}, & \text{for unlike} - \text{particle collisions} \\ \dfrac{n_a}{2N_{cn}/N_a}, & \text{for like} - \text{particle collisions,} \end{cases}$$

where $n_a$ ( $n_b$ ) and $N_a$ ( $N_b$ ) are, respectively, the density and model particle number of the species that particle $a$ ( $b$ ) belongs to, and $N_{cn}$ is the like particle collision number in the time interval $\Delta t$. The developed nonlinear collision operator ensures the conservations of particle number, momentum and energy, and is equivalent to the exact Fokker-Planck operator by correctly reproducing the friction coefficient and the diffusion tensor. The highly vectorized algorithm has been designed for fast implementation of the operator. This nonlinear operator is employed in the present model.

At the steady state, the electron particle flux balance and energy flux balance are obtained from the zeroth and second moment of Eq.(6), which are given by, respectively,

$$\dot{S}_e = (1 - \delta_e) \int \frac{f_e}{\tau_{\|e}} H(|\vec{v}_\|| - v_c) d^3v, \tag{15}$$

$$\frac{3}{2}\dot{S}_e T_{se} + \frac{3}{2}\dot{S}_{qe}(T_{se} - T_e) + \delta_e \frac{1}{2} m_e v_c^2 \int \frac{f_e}{\tau_{\|e}} H(|\vec{v}_\|| - v_c) d^3v = \int \frac{1}{2} m_e v^2 \frac{f_e}{\tau_{\|e}} H(|\vec{v}_\|| - v_c) d^3v. \tag{16}$$

The physical meaning of each term is evident. The balance relations for ions can be obtained from Eq.(7).

To obtain self-consistent sheath potential, one usually needs solving Poisson's equation. In the SOL (including presheath region ), the charge neutrality, i.e,

$$n_e = n_i \tag{17}$$

is a good approximation to the solution of Poisson's equation, except when one wants to obtain the detail spatial structure of the sheaths very adjacent to the divertor plates. In this study, the self-consistent sheath potential $\Phi$ (exactly saying, the total potential drop of the sheath) is obtained by employing the neutrality constraint. This is also consistent with the fact that the model is established in the velocity space, neglecting the sheath structure.

The Eq.(6) and Eq.(7) are solved by Monte Carlo particle simulation to obtain the steady state solution under the constraint of the neutrality, Eq.(17). We neglect electron-ion collisions for numerical simplicity and reduction of simulation cost, thus we can solve

the two equations separately. One may notice that the potential $\Phi$ does not enter Eq.(7) in determining the behavior of ions. This results from that the potential is approximated as the square well in the model. ( The Debye sheaths are assumed to be infinitely thin compared to the parallel dimension of the SOL. )

# 3. COLLISIONAL SOL PLASMA

The Monte Carlo simulation model presented in the previous section can hold for arbitrary collisionality. However, in this section, we apply the model only to the collisional SOL plasma ( $L/(2\lambda_a) > 1$ ) and compare the calculation results with theoretical predictions to confirm the validity of the model.

Simulations are performed by following procedures. First, we solve the equation for ions given by Eq.(7) to obtain ion distribution function at the steady state. A large number of ions with an arbitrary velocity distribution are initially loaded in the system, and then followed according to Eq.(7) until the steady state is reached. Next, we solve, by the same way as for ions, the Fokker-Planck equation for electrons, Eq.(6), with a specified potential $\Phi$ to obtain the electron distribution function at steady state. Equation (6) is repeatedly solved changing $\Phi$ until the neutrality constraint is satisfied; $n_e = n_i$. The important point is that the steady-state solutions to Eq.(6) and Eq.(7) must be unique. A series of test simulations are carried out, which indeed show that the steady-state solution does not depend on the evolving history of the simulation system and initial distribution function of loaded particles. This ensures that one can obtain the physically reasonable steady state by imposing the neutrality constraint.

The input parameters are listed in Table I, where the total particle fluxes across the separatrix into the SOL, source temperatures, the SOL volume, as well as the induced input power are selected to be close to those of JT-60U [26]. The large length of magnetic field line is used in order to make the SOL plasma to be collisional. The simulations are performed by varying the emission rate of secondary electrons. For normalization, time scale $\tau_s$ and a density scale $n_s$ are defined by the relations,

$$\dot{S}_i = \frac{n_s}{\tau_s} \quad \text{and} \quad \tau_s = \frac{3\sqrt{m_e}T_s^{3/2}}{4\sqrt{\pi}e^4 n_s \ln\Lambda}.$$

The time evolutions of ion temperatures and density are shown in Fig. 2, which gives the final steady state with $T_{i\perp}/T_{si} = 0.811$, $T_{i\parallel}/T_{si} = 0.668$, and $n_i/n_s = 9.40$. The

perpendicular and parallel temperature are separated, and both are lower than the source temperature. The parallel temperature is decreased because the energetic ions in the tail of the distribution are easily lost to the plates, while the perpendicular temperature is reduced via collisional energy transport to the parallel component.

The same diagrams for electrons obtained by the simulation run with $\delta_e = 0.8$ are shown in Fig. 3(a) and (b), in which the steady state satisfies the neutrality constraint, $n_e \approx n_i$. Figures 3(c) and (d) show the electron velocity distribution at the steady state. The circular contour plot (Fig. 3(d)) implies that the electron distribution is nearly isotropic, while Fig. 3(c) shows that the distribution in the parallel direction is close to the Maxwellian of the same temperature as $T_{e\|}$ (shown by the dash line). Thus, one can conclude that the electron distribution is close to a Maxwellian. Because the electron mean-free path is shorter than the system length ( $2\lambda_e/L = 0.132$ ), the electrons are sufficiently isothermalized.

The influence of secondary electron emission on the steady-state SOL plasma is investigated by the simulation, and the results are presented in Fig. 4. The normalized electron temperatures $T_{e\perp}/T_s$ and $T_{e\|}/T_s$ (Fig. 4(a)), the electron collisionality $L/(2\lambda_e)$ (Fig. 4(b)), the normalized sheath potentials $-e\Phi/T_e$ and $-e\Phi/T_s$ (Fig. 4(c)), and the electron sheath energy transmission factor $\gamma_e$ (Fig. 4(d)) are shown as functions of the secondary electron emission rate. ( Note that the secondary electron emission has no influence on the ions in the model ).

The secondary electrons emitted from the plates enter the SOL with small perpendicular energy of a few $eV$. In the collisional case, the secondary electrons will significantly cool the warm electrons flowing into the SOL from the confinement region. As the emission is increased, the electron temperatures are decreased, as shown in Fig. 4(a). Correspondingly, the electrons become more collisional (see Fig. 4(b) ), and more isothermal. This can be seen from Fig. 4(a) where the differences between $T_{e\perp}$ and $T_{e\|}$ are decreased as $\delta_e$ is increased. Figure 4(c) shows that the magnitude of the sheath potential ( solid square ) is decreased as the secondary electron emission rate is increased. The potential $\Phi$ does not enter Eq.(7) to affect ion behaviors including ion flux onto the plate. As particle fluxes for electrons and ions onto the plate should be ambipolar, the variations in $\Phi$ also have no effect on the total electron flux onto the plate. When the secondary electron emission is increased, the primary electron flux must increase to maintain a constant total flux. This

requires a reduction of the potential to enhance the number of untrapped electrons.

The simulation results are compared with those of analytical models[4,14]. Kinetic models proposed so far do not include secondary electrons. Thus the comparison is difficult between the kinetic models and the present simulation. The isothermal fluid model in Ref. 14 assumes that ions flow through the plasma-sheath interface at the acoustic speed and that electrons obey a Maxwell-Boltzmann distribution. The model is available to collisional SOL plasma on which the present simulations are performed. It gives the floating potential drop $\Psi_f$ as

$$\frac{e\Psi_f}{T_e} = \frac{1}{2}\ln[(2\pi\frac{m_e}{m_i})(1+\frac{T_i}{T_e})(1-\delta_e)^{-2}] \tag{18}$$

The potentials given by Eq.(18) are plotted in Fig. 4(c) ( solid triangles ). Note that the floating potential $\Psi_f$ is not the potential $\Phi$ in our simulations. The total potential drop $\Phi$ is the sum of floating potential and presheath potential if the spatial structure of a general Debye sheath is considered. The presheath drop from the fluid model is

$$\frac{e\Psi_{ps}}{T_e} = -\ln(2+\frac{V_0}{c_s}), \tag{19}$$

where $V_0$ and $c_s$ are the ion initial mean speed ( the speed at the point far from the plasma-sheath interface ) and the ion acoustic speed, respectively. In the case of present simulation, it gives $e\Psi_{ps}/T_e = -0.69$. The potentials evaluated by $(\Psi_f + \Psi_{ps})$ are also drawn in Fig. 4(c) (blank triangles ), which are in reasonable agreement with the simulation results ( blank squares ).

The electron sheath energy transmission factors are compared with those obtained from simple analyses of energy balance [4,14]. The analyses are briefly reviewed to extend the floating sheath to the entire sheath.

In the presence of the sheath, the SOL electrons lose energy at the power density rate ( the loss energy flux )

$$P_e = \Gamma_{e0}^{loss} 2T_e - \Gamma_i^{loss} e\Phi, \tag{20}$$

where $\Gamma_i^{loss}$ is the loss flux of ions, and $\Gamma_{e0}^{loss} = \frac{1}{1-\delta_e}\Gamma_i^{loss}$ is the primary loss flux of electrons. The factor of two in the first term of Eq.(20) results from the assumption of Maxwellian electrons, while the last term is due to the fact that only electrons with energies greater than the sheath potential can penetrate the barrier onto the plates, and represents the energy transferred from electrons to ions in the sheath field. The emitted

secondary electron energy is neglected since it is typically a few $eV$. The electron sheath transmission factor is defined as

$$\gamma_e \equiv \frac{P_e}{T_e \Gamma_i^{loss}} = \frac{2}{1-\delta_e} - \frac{e\Phi}{T_e}. \tag{21}$$

In the present simulation model, there is no impurity radiation loss so that

$$Q_e^{in} = Q_e^{loss} = \gamma_e \Gamma_i^t T_e,$$

which gives

$$\gamma_e = \frac{3}{2}\frac{T_s}{T_e} + \frac{3}{2}\frac{\dot{S}_{qe}}{\dot{S}_i}\left(\frac{T_s}{T_e} - 1\right). \tag{22}$$

This provides the evaluation of the electron sheath energy transmission factor in the simulations. In the calculation $\gamma_e$ by Eq.(21), the normalized potential energies $-e\Phi/T_e$ are evaluated either from the simulation results or by $-\frac{e(\Psi_f + \Psi_{ps})}{T_e}$ via Eqs.(18) and (19). We refer the former to Theory 1 and latter to Theory 2. It is obviously seen from Fig. 4(d) that numerical values for $\gamma_e$ calculated based on the present model are in good agreement with both Theory 1 and Theory 2.

The simulation results shown above have been obtained under fixed $\dot{S}_{qe}$ ($\dot{S}_{qe} = 3.0\dot{S}_i$). The simulations with $\delta_e = 0.5$ have been performed as well, varying only $\dot{S}_{qe}$ over the range $\dot{S}_i \leq \dot{S}_{qe} \leq 5.0\dot{S}_i$. These simulations give the same conclusion, i.e, the numerical values of total potential drop $-e\Phi/T_e$ and electron sheath energy transmission factor $\gamma_e$ are in close agreement with the analytic predictions.

# 4. SUMMARY

A new Monte Carlo model has been presented for the study of the steady-state SOL plasma. The ion distribution function, as well as the electron distribution function which was usually assumed to be the Maxwellian in the previous models, have been obtained by solving the Fokker-Planck equation with the Monte Carlo method. The model established in the velocity space includes sources and sinks to describe the incoming fluxes and outgoing fluxes. The conductive heat flux from the confinement region has newly been introduced to represent actual overall energy balance more precisely in the SOL. The secondary electron emission can be readily included in the model. Coulomb collisions have been accurately implemented by the nonlinear Monte Carlo collision operator. Under above considerations, the model is appropriate to give important features of the SOL

plasma in the entire range of collisionality, consistently with the main plasma parameters near the separatrix.

To confirm the validity of the proposed model, simulations have been performed for collisional SOL plasma and compared with the theories. Dependences of electron temperature and collisionality, total sheath potential drop and electron sheath energy transmission factor on the emission rate of secondary electrons have been shown. The total potential drop and electron sheath energy transmission factor obtained from the simulations agree close with the analytic predictions and the validity of the proposed model has been confirmed.

An immediate and important application of the model is to investigate a collisionless plasma in the high temperature operation mode of the SOL. The simulation study using the present model can clarify the influence of secondary electron emission on the characteristics of so-called high temperature divertor plasma. Within the present framework, the model can be extended to include other effects, such as neutral recycling by introducing a new source of the neutral particle emission. These works are currently in progress.

## ACKNOWLEDGEMENTS

One of the authors ( W. X. Wang ) would like to acknowledge hospitality of the Theory and Data Analysis Division of The National Institute for Fusion Science ( NIFS ). He also thanks professor T. Q. Chang for his support and encouragement. He is supported by the Japanese Ministry of Education, Science and Culture ( MONBUSHO ). Numerical calculations were carried out by using the super computer SX-3 of NIFS.

## REFERENCES


[1] LANGMUIR, I., Phys. Rev. **33** (1929) 945.

[2] TONKS, L., LANGMUIR, I., Phys. Rev. **34** (1929) 876.

[3] OHYABU, N., et al., Nucl. Fusion **34** (1994) 387.

[4] HOBBS, G.D., WESSON, J.A., Plasma Phys. **9** (1967) 85.

[5] HINTON, F.L., HAZELTINE, R.D., Phys. Fluids **17** (1974) 2236.

[6] BAILEY, A.W., EMMERT, G.A., Nucl. Fusion **24** (1984) 1439.

[7] CATTO, P.J., HAZELTINE, R.D., Phys. Plasmas **1** (1994) 1882.

[8] HELANDER, P., CATTO, P.J., Phys. Plasmas **1** (1994) 2213.

[9] EMMERT, G.A., et al., Phys. Fluids **23** (1980) 803.

[10] BISSELL, R.C., JOHNSON, P.C., Phys. Fluids **30** (1987) 779.

[11] RIEMANN, K.-U., Phys. Fluids **24** (1981) 2163.

[12] BIEHLER, S., et al., Phys. Fluids **31** (1988) 1999.

[13] ANDREWS, J.G., STANGEBY, P.C., J. Phys., A **3** (1970) L39.

[14] STANGEBY, P.C., Phys. Fluids **27** (1984) 682.

[15] BISSELL, R.C., et al., Phys. Fluids B **1** (1989) 1133.

[16] McCULLEN, J.D., et al., Phys. Fluids B **1** (1989) 448.

[17] KOCH, D.J., HITCHON, W.N.G., Phys. Fluids B **1** (1989) 2239.

[18] MONTIERTH, L.M., et al., Phys. Fluids B **1** (1989) 1911.

[19] PROCASSINI, R.J., BIRSALL, C.K., Phys. Fluids B **3** (1991) 1876.

[20] PROCASSINI, R.J., et al., Nucl. Fusion **30** (1990) 2329.

[21] TAKIZUKA,T., et al., J. Nucl. Mater. **128&129** (1984) 104.

[22] WANG, W.X., et al., *"An Accurate Nonlinear Monte Carlo Collision operator"*, Research Report of The National Institute for Fusion Science, NIFS-**345**, March 1995 ( submitted to J. Comput. Phys.).

[23] LANDAU, L.D., ZhETF (J. Exptl. Theoret. Phys.) **7** (1937) 203.

[24] KATANUMA, I., et al., J. Phys. Soc. Japan **62** (1993) 3446.

[25] HINTON, F.L., in Handbook of Plasma Physics (ROSENBLUTH, M.N., SAGDEEV, R.Z., Ed.), Vol. 1, North-Holland Publishing Company, Amsterdam (1983) 147.

[26] KONOSHIMA, S., TOI, K., J. Plasma and Fusion Res. **71** (1995) 109.

## Figure Captions

**Fig. 1** A schematic representation of one dimensional SOL system.

**Fig. 2** The time evolution of ions: (a) ion temperature ( parallel temperature $T_{\parallel} = T_z$ and perpendicular temperature $T_{\perp} = (T_x + T_y)/2 \simeq T_x \simeq T_y$ ), (b) ion density of the simulation system.

**Fig. 3** The time evolution and the steady-state distribution function of electrons obtained from the simulation with $\delta_e = 0.8$: (a) electron temperature, (b) density, (c) parallel distribution function ( the dotted lines denote the positions of $|\vec{v_{\parallel}}| = v_c \equiv \sqrt{-2e\Phi/m_e}$ and the dashed line shows the Maxwellian distribution with the same temperature ), (d) contour plot of the distribution function.

**Fig. 4** Dependences on the emission rate of secondary electrons $\delta_e$ obtained from the simulation: (a) the electron temperature, (b) the collisionality $L/(2\lambda_e)$, (c) the sheath potential drop ( blank squares: $-e\Phi/T_e$ and solid squares: $-e\Phi/T_s$ ), and (d) the electron sheath energy transmission factor ( blank circles ); for comparison, also plotted are the analytic predictions of (c) the sheath potential drops $-\Psi_f/T_e$ ( solid triangles ) and $-(\Psi_f + \Psi_{ps})/T_e$ (blank triangles ), and (d) the electron sheath energy transmission factor given by Eq.(21) where $-e\Phi/T_e$ is measured from the simulation ( blank triangles referred as Theory 1 ) and evaluated via $-(\Psi_f + \Psi_{ps})/T_e$ ( blank squares referred as Theory 2 ).

TABLE I. PARAMETERS USED TO MODEL COLLISIONAL SOL PLASMA

| | |
|---|---|
| Total particle fluxes | $\Gamma_e^t = \Gamma_i^t = 6.0 \times 10^{21}$ sec$^{-1}$ |
| Source temperatures | $T_{se} = T_{si} = T_s = 2.0$ keV |
| SOL volume | $V_{SOL} = 0.5$ m$^3$ |
| Magnetic field line length | $L = 2450.0$ m |
| Electron exchange rate | $\dot{S}_{qe} = 3.0\dot{S}_i$ $= 3.6 \times 10^{22}$ sec$^{-1} \cdot$ m$^{-3}$ |
| Ion exchange rate | $\dot{S}_{qi} = 0.0$ |
| Secondary electron emission rate | $\delta_e = 0.0,\ 0.5,\ 0.8$ |
| Perpendicular temperature of secondary electrons | $T_{2e\perp} = 1.0$ eV |

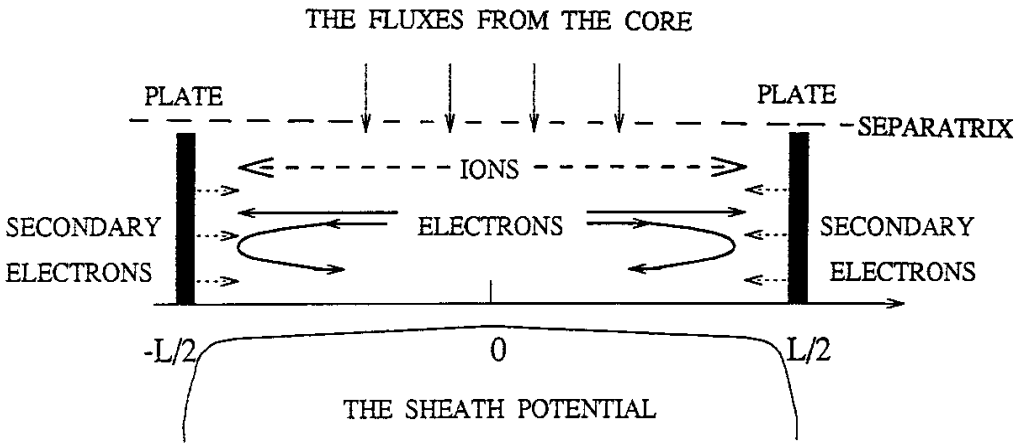
THE FLUXES FROM THE CORE
PLATE
PLATE
SEPARATRIX
IONS
SECONDARY
ELECTRONS
ELECTRONS
SECONDARY
ELECTRONS
-L/2
0
L/2
THE SHEATH POTENTIAL

Fig. 1

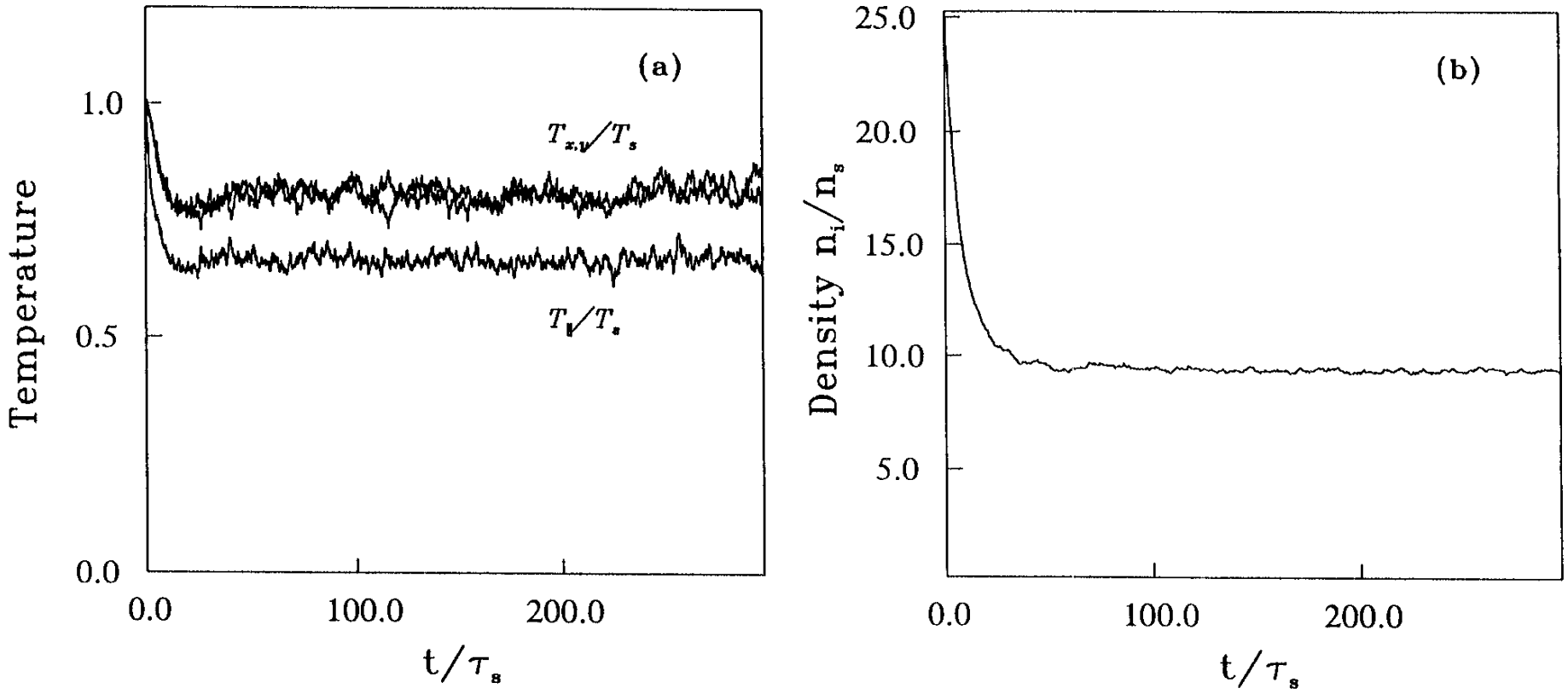
(a)
1.0
0.5
0.0
Temperature
$T_{x,y}/T_s$
$T_{\parallel}/T_s$
0.0
100.0
200.0
$t/\tau_s$
(b)
25.0
20.0
15.0
10.0
5.0
Density $n_i/n_s$
0.0
100.0
200.0
$t/\tau_s$

Fig. 2

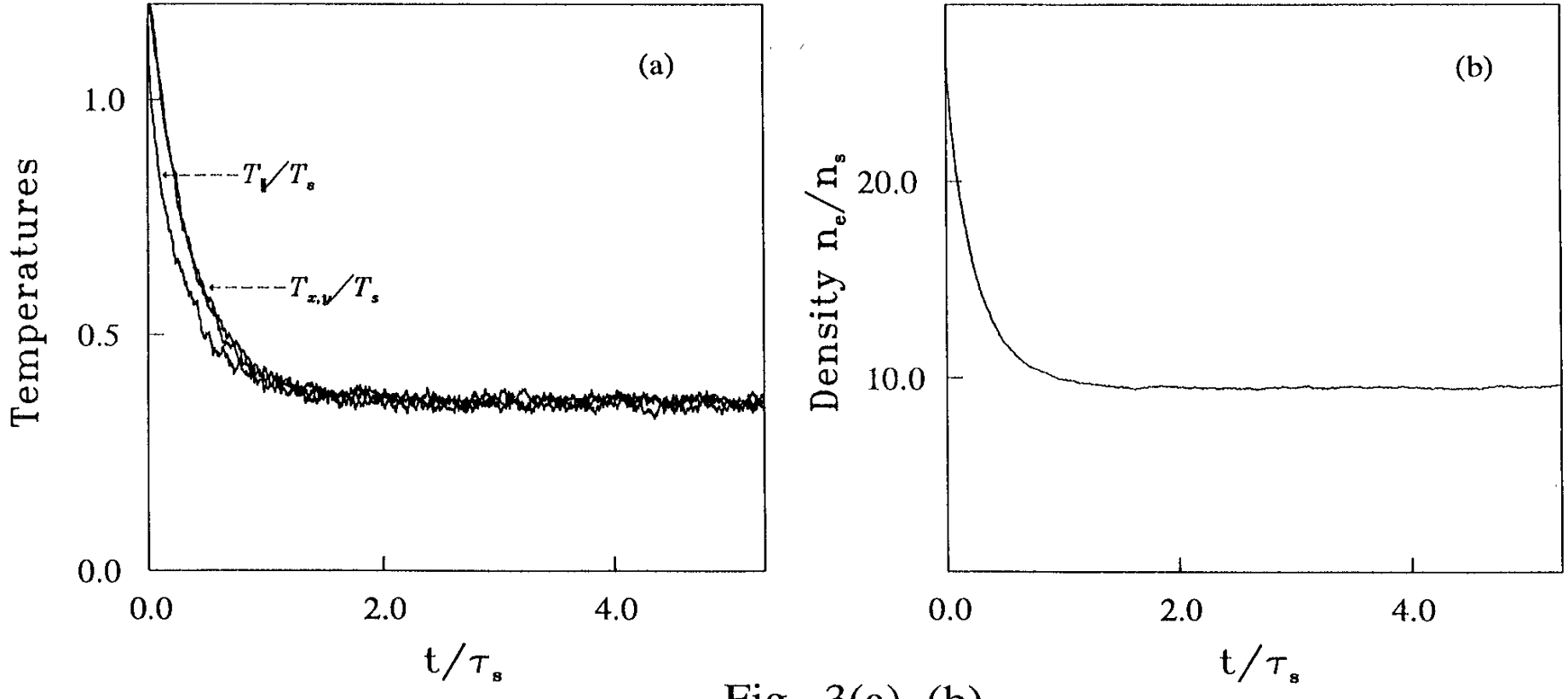
(a)
Temperatures
1.0
0.5
0.0
$T_\parallel/T_s$
$T_{x,y}/T_s$
0.0
2.0
4.0
$t/\tau_s$
(b)
Density $n_e/n_s$
20.0
10.0
0.0
2.0
4.0
$t/\tau_s$

Fig. 3(a), (b)

Fig. 3(c)

The Distribution Function

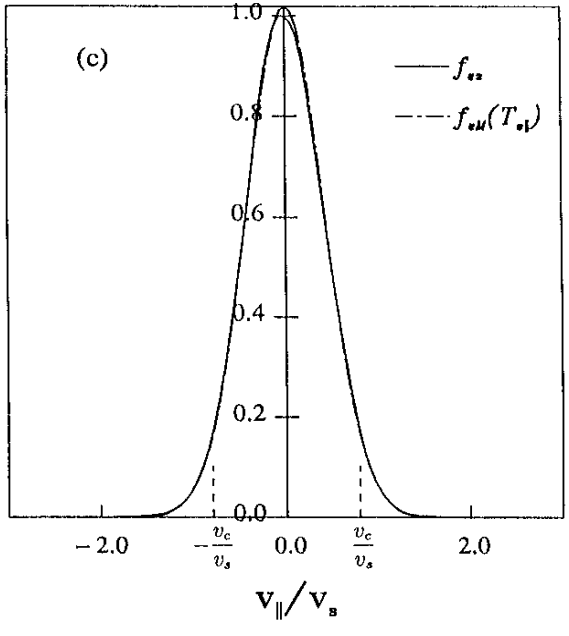


Fig. 3(d)

The Contour of Distribution Function

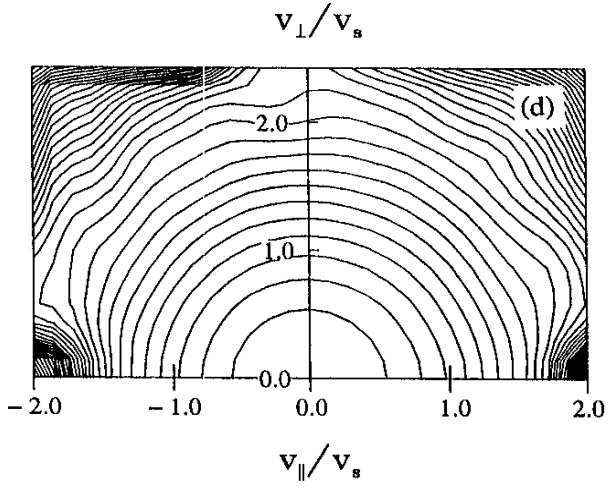

Fig. 4(a),(b)

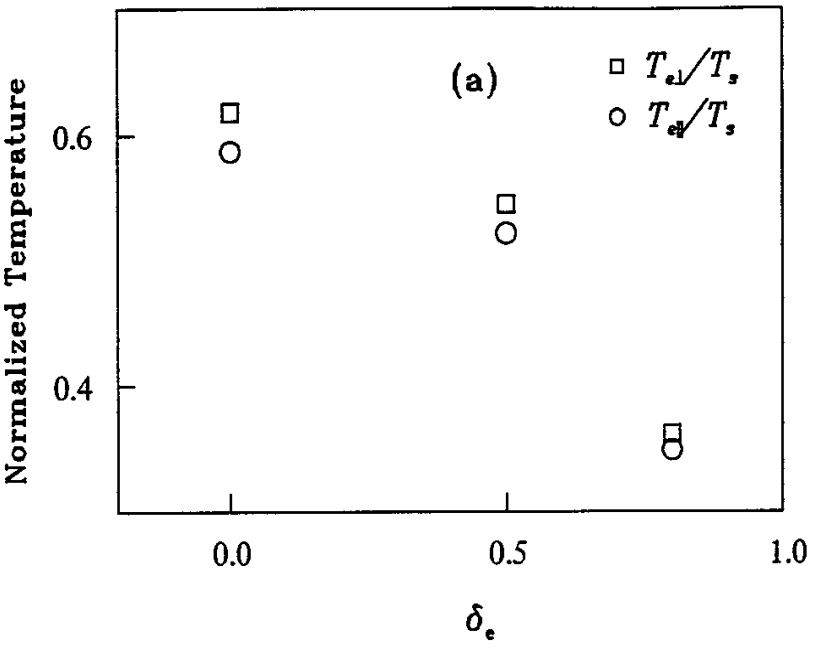
(a)
$T_{e\perp}/T_s$
$T_{e\parallel}/T_s$
Normalized Temperature
0.6
0.4
0.0
0.5
1.0
$\delta_e$

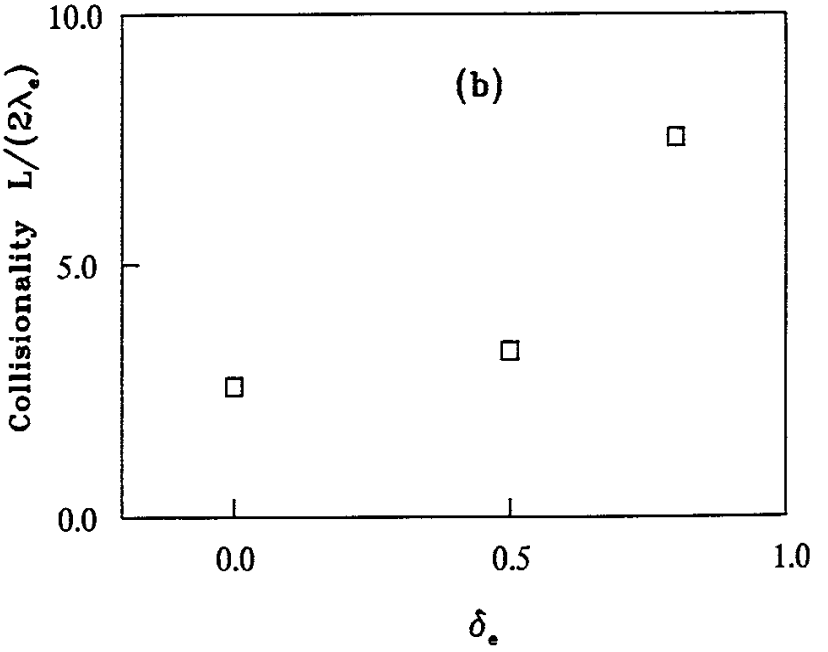
(b)
Collisionality $L/(2\lambda_e)$
10.0
5.0
0.0
0.0
0.5
1.0
$\delta_e$

Fig. 4(c),(d)

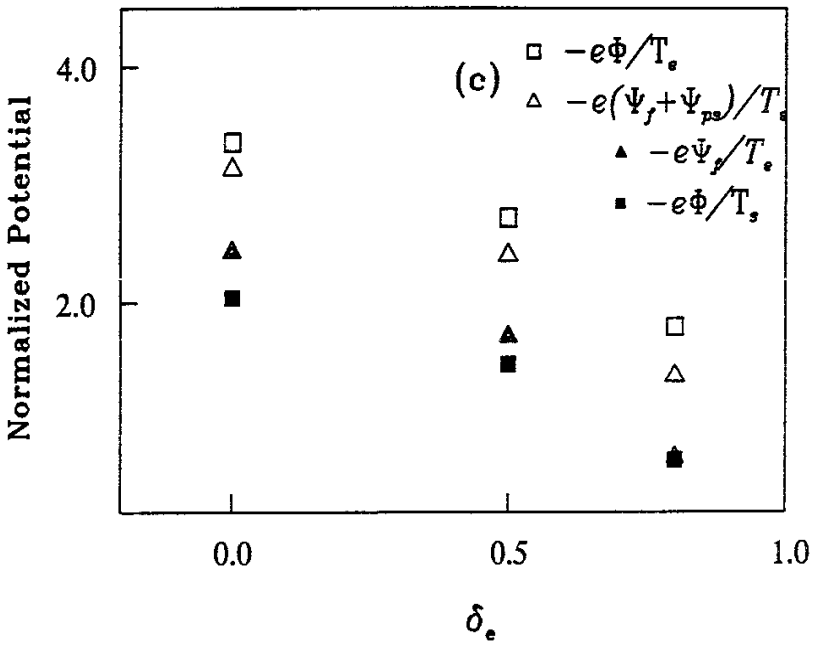
Normalized Potential
4.0
2.0
(c)
$-e\Phi/T_e$
$-e(\Psi_f+\Psi_{ps})/T_e$
$-e\Psi_f/T_e$
$-e\Phi/T_s$
0.0
0.5
1.0
$\delta_e$

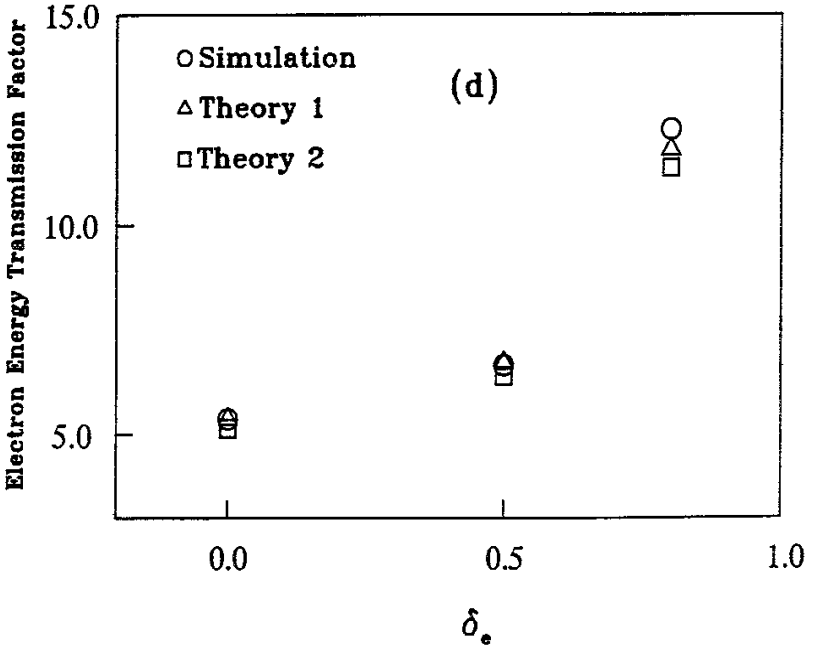
Electron Energy Transmission Factor
15.0
10.0
5.0
Simulation
Theory 1
Theory 2
(d)
0.0
0.5
1.0
$\delta_e$

## Recent Issues of NIFS Series

NIFS-343 A. Ejiri, S. Sakakibara and K. Kawahata,
*Signal Based Mixing Analysis for the Magnetohydrodynamic Mode Reconstruction from Homodyne Microwave Reflectometry*; Mar.. 1995

NIFS-344 B.B.Kadomtsev, K. Itoh, S.-I. Itoh
*Fast Change in Core Transport after L-H Transition*; Mar. 1995

NIFS-345 W.X. Wang, M. Okamoto, N. Nakajima and S. Murakami,
*An Accurate Nonlinear Monte Carlo Collision Operator*; Mar. 1995

NIFS-346 S. Sasaki, S. Takamura, S. Masuzaki, S. Watanabe, T. Kato, K. Kadota,
*Helium I Line Intensity Ratios in a Plasma for the Diagnostics of Fusion Edge Plasmas*; Mar. 1995

NIFS-347 M. Osakabe,
*Measurement of Neutron Energy on D-T Fusion Plasma Experiments;* Apr. 1995

NIFS-348 M. Sita Janaki, M.R. Gupta and Brahmananda Dasgupta,
*Adiabatic Electron Acceleration in a Cnoidal Wave;* Apr. 1995

NIFS-349 J. Xu, K. Ida and J. Fujita,
*A Note for Pitch Angle Measurement of Magnetic Field in a Toroidal Plasma Using Motional Stark Effect*; Apr. 1995

NIFS-350 J. Uramoto,
*Characteristics for Metal Plate Penetration of a Low Energy Negative Muonlike or Pionlike Particle Beam*: Apr. 1995

NIFS-351 J. Uramoto,
*An Estimation of Life Time for A Low Energy Negative Pionlike Particle Beam:* Apr. 1995

NIFS-352 A. Taniike,
*Energy Loss Mechanism of a Gold Ion Beam on a Tandem Acceleration System:* May 1995

NIFS-353 A. Nishizawa, Y. Hamada, Y. Kawasumi and H. Iguchi,
*Increase of Lifetime of Thallium Zeolite Ion Source for Single-Ended Accelerator*: May 1995

NIFS-354 S. Murakami, N. Nakajima, S. Okamura and M. Okamoto,
*Orbital Aspects of Reachable $\beta$ Value in NBI Heated Heliotron/Torsatrons;* May 1995

NIFS-355 H. Sugama and W. Horton,

*Neoclassical and Anomalous Transport in Axisymmetric Toroidal Plasmas with Electrostatic Turbulence*; May 1995

NIFS-356 N. Ohyabu
*A New Boundary Control Scheme for Simultaneous Achievement of H-mode and Radiative Cooling (SHC Boundary);* May 1995

NIFS-357 Y. Hamada, K.N. Sato, H. Sakakita, A. Nishizawa, Y. Kawasumi, R. Liang, K. Kawahata, A. Ejiri, K. Toi, K. Narihara, K. Sato, T. Seki, H. Iguchi, A. Fujisawa, K. Adachi, S. Hidekuma, S. Hirokura, K. Ida, M. Kojima, J. Koong, R. Kumazawa, H. Kuramoto, T. Minami,. M. Sasao, T. Tsuzuki, J.Xu, I. Yamada, and T. Watari,
*Large Potential Change Induced by Pellet Injection in JIPP T-IIU Tokamak Plasmas;* May 1995

NIFS-358 M. Ida and T. Yabe,
*Implicit CIP (Cubic-Interpolated Propagation) Method in One Dimension*; May 1995

NIFS-359 A. Kageyama, T. Sato and The Complexity Simulation Group,
*Computer Has Solved A Historical Puzzle: Generation of Earth's Dipole Field*; June 1995

NIFS-360 K. Itoh, S.-I. Itoh, M. Yagi and A. Fukuyama,
*Dynamic Structure in Self-Sustained Turbulence*; June 1995

NIFS-361 K. Kamada, H. Kinoshita and H. Takahashi,
*Anomalous Heat Evolution of Deuteron Implanted Al on Electron Bombardment*; June 1995

NIFS-362 V.D. Pustovitov,
*Suppression of Pfirsch-schlüter Current by Vertical Magnetic Field in Stellarators;* June 1995

NIFS-363 A. Ida, H. Sanuki and J. Todoroki
*An Extended K-dV Equation for Nonlinear Magnetosonic Wave in a Multi-Ion Plasma*; June 1995

NIFS-364 H. Sugama and W. Horton
*Entropy Production and Onsager Symmetry in Neoclassical Transport Processes of Toroidal Plasmas;* July 1995

NIFS-365 K. Itoh, S.-I. Itoh, A. Fukuyama and M. Yagi,
*On the Minimum Circulating Power of Steady State Tokamaks*; July 1995

NIFS-366 K. Itoh and Sanae-I. Itoh,
*The Role of Electric Field in Confinement*; July 1995

NIFS-367 F. Xiao and T. Yabe,

*A Rational Function Based Scheme for Solving Advection Equation;* July 1995

NIFS-368 Y. Takeiri, O. Kaneko, Y. Oka, K. Tsumori, E. Asano, R. Akiyama, T. Kawamoto and T. Kuroda,
*Multi-Beamlet Focusing of Intense Negative Ion Beams by Aperture Displacement Technique;* Aug. 1995

NIFS-369 A. Ando, Y. Takeiri, O. Kaneko, Y. Oka, K. Tsumori, E. Asano, T. Kawamoto, R. Akiyama and T. Kuroda,
*Experiments of an Intense H- Ion Beam Acceleration*; Aug. 1995

NIFS-370 M. Sasao, A. Taniike, I. Nomura, M. Wada, H. Yamaoka and M. Sato,
*Development of Diagnostic Beams for Alpha Particle Measurement on ITER*; Aug. 1995

NIFS-371 S. Yamaguchi, J. Yamamoto and O. Motojima;
*A New Cable -in conduit Conductor Magnet with Insulated Strands*; Sep. 1995

NIFS-372 H. Miura,
*Enstrophy Generation in a Shock-Dominated Turbulence*; Sep. 1995

NIFS-373 M. Natsir, A. Sagara, K. Tsuzuki, B. Tsuchiya, Y. Hasegawa, O. Motojima,
*Control of Discharge Conditions to Reduce Hydrogen Content in Low Z Films Produced with DC Glow;* Sep. 1995

NIFS-374 K. Tsuzuki, M. Natsir, N. Inoue, A. Sagara, N. Noda, O. Motojima, T. Mochizuki, I. Fujita, T. Hino and T. Yamashina,
*Behavior of Hydrogen Atoms in Boron Films during $H_2$ and He Glow Discharge and Thermal Desorption;* Sep. 1995

NIFS-375 U. Stroth, M. Murakami, R.A. Dory, H. Yamada, S. Okamura, F. Sano and T. Obiki,
*Energy Confinement Scaling from the International Stellarator Database*; Sep. 1995

NIFS-376 S. Bazdenkov, T. Sato, K. Watanabe and The Complexity Simulation Group,
*Multi-Scale Semi-Ideal Magnetohydrodynamics of a Tokamak Plasma;* Sep. 1995

NIFS-377 J. Uramoto,
*Extraction of Negative Pionlike Particles from a H2 or D2 Gas Discharge Plasma in Magnetic Field;* Sep. 1995

NIFS-378 K. Akaishi,
*Theoretical Consideration for the Outgassing Characteristics of an Unbaked Vacuum System*; Oct. 1995

NIFS-379 H. Shimazu, S. Machida and M. Tanaka,
*Macro-Particle Simulation of Collisionless Parallel Shocks*; Oct. 1995

NIFS-380 N. Kondo and Y. Kondoh,
*Eigenfunction Spectrum Analysis for Self-organization in Dissipative Solitons;* Oct. 1995

NIFS-381 Y. Kondoh, M. Yoshizawa, A. Nakano and T. Yabe,
*Self-organization of Two-dimensional Incompressible Viscous Flow in a Friction-free Box;* Oct. 1995

NIFS-382 Y.N. Nejoh and H. Sanuki,
*The Effects of the Beam and Ion Temperatures on Ion-Acoustic Waves in an Electron Beam-Plasma System;* Oct. 1995

NIFS-383 K. Ichiguchi, O. Motojima, K. Yamazaki, N. Nakajima and M. Okamoto
*Flexibility of LHD Configuration with Multi-Layer Helical Coils;*
Nov. 1995

NIFS-384 D. Biskamp, E. Schwarz and J.F. Drake,
*Two-dimensional Electron Magnetohydrodynamic Turbulence*; Nov. 1995

NIFS-385 H. Kitabata, T. Hayashi, T. Sato and Complexity Simulation Group,
*Impulsive Nature in Collisional Driven Reconnection*; Nov. 1995

NIFS-386 Y. Katoh, T. Muroga, A. Kohyama, R.E. Stoller, C. Namba and O. Motojima,
*Rate Theory Modeling of Defect Evolution under Cascade Damage Conditions:The Influence of Vacancy-type Cascade Remnants and Application to the Defect Production Chracterization by Microstructural Analysis;* Nov. 1995

NIFS-387 K. Araki, S. Yanase and J. Mizushima,
*Symmetry Breaking by Differential Rotation and Saddle-node Bifurcation of the Thermal Convection in a Spherical Shell*; Dec. 1995

NIFS-388 V.D. Pustovitov,
*Control of Pfirsch-Schlüter Current by External Poloidal Magnetic Field in Conventional Stellarators:* Dec. 1995

NIFS-389 K. Akaishi,
*On the Outgassing Rate Versus Time Characteristics in the Pump-down of an Unbaked Vacuum System*; Dec. 1995

NIFS-390 K.N. Sato, S. Murakami, N. Nakajima, K. Itoh,
*Possibility of Simulation Experiments for Fast Particle Physics in Large Helical Device (LHD)*; Dec. 1995